5-12-2004

Tyrosine B10 Inhibits Stabilization of Bound Carbon Monoxide and Oxygen in Soybean Leghemoglobin

Suman Kundu
Iowa State UniVersity, Ames, Iowa

George C. Blouin
Rice UniVersity, Houston, Texas

Scott A. Premer

Gautam Sarath
University of Nebraska-Lincoln, Gautam.sarath@ars.usda.gov

John S. Olson
Rice University, olson@rice.edu

See next page for additional authors

Authors

Suman Kundu, George C. Blouin, Scott A. Premer, Gautam Sarath, John S. Olson, and Mark S. Hargrove

Tyrosine B10 Inhibits Stabilization of Bound Carbon Monoxide and Oxygen in Soybean Leghemoglobin[†]

Suman Kundu,[‡] George C. Blouin,[§] Scott A. Premer,[‡] Gautam Sarath,[⊥] John S. Olson,[§] and Mark S. Hargrove*,[‡]

*Department of Biochemistry, Biophysics and Molecular Biology, Iowa State University, Ames, Iowa 50011,
Department of Biochemistry and Cell Biology and the W. M. Keck Center for Computational Biology, Rice University,
Houston, Texas 77005, and U.S. Department of Agriculture and University of Nebraska, Lincoln, Nebraska 68502*

ABSTRACT: Detailed comparisons of the carbon monoxide FTIR spectra and ligand-binding properties of a library of E7, E11, and B10 mutants indicate significant differences in the role of electrostatic interactions in the distal pockets of wild-type sperm whale myoglobin and soybean leghemoglobin. In myoglobin, strong hydrogen bonds from several closely related conformations of the distal histidine (His[E7]) side chain preferentially stabilize bound oxygen. In leghemoglobin, the imidazole side chain of His[E7] is confined to a single conformation, which only weakly hydrogen bonds to bound ligands. The phenol side chain of Tyr[B10] appears to "fix" the position of His[E7], probably by donating a hydrogen bond to the Nδ atom of the imidazole side chain. The proximal pocket of leghemoglobin is designed to favor strong coordination bonds between the heme iron and axial ligands. Thus, high oxygen affinity in leghemoglobin is established by a favorable staggered geometry of the proximal histidine. The interaction between His[E7] and Tyr[B10] prevents overstabilization of bound oxygen. If hydrogen bonding from His[E7] were as strong as it is in mammalian myoglobin, the resultant ultrahigh affinity of leghemoglobin would prevent oxygen transport in root nodules.

Myoglobin (Mb[1]) and leghemoglobin (Lb) perform similar physiological roles in their respective environments. Both facilitate the diffusion of oxygen by increasing its effective concentration in either muscle (Mb) or root nodule (Lb) tissue. Each protein exhibits the requisite rate constants for transport, but Lb has a 20-fold higher affinity for oxygen because it must maintain lower free oxygen concentrations to prevent inhibition of the nitrogenase complex in the root nodule (*1*, *2*). The two proteins share a globin fold that originally led to the assumption that they function similarly at the molecular level (*3*). However, recent detailed studies of soybean leghemoglobin (Lba) indicate that it uses a mechanism to regulate ligand binding distinct from that of Mb (*4−9*).

Mutagenesis studies have shown that proximal contributions to O$_2$ affinity are quite different in Lba compared to those in sperm whale Mb (*6*). In Lba, the plane of the His[F8] imidazole side chain is staggered with respect to the pyrrole nitrogen atoms of the porphyrin ring. This orientation favors in-plane movement of the iron atom and strong axial ligand coordination. In all mammalian Mbs, the His[F8] side chain is in an eclipsed geometry that inhibits ligand coordination (*10−12*). These ideas were confirmed directly by swapping the F helices between Lba and sperm whale Mb (*6*). Thus, both stereochemical arguments and direct experimental measurements show that the Lba proximal heme pocket favors high oxygen affinity.

Stabilization of bound ligands by hydrogen bonding in the distal pocket of Lba is weakened to prevent an ultrahigh O$_2$ affinity that would inhibit transport in root nodules. This idea is supported by comparative mutagenesis experiments with recombinant Lbs and Mbs containing altered distal pockets (*4*, *5*, *13−15*). His[E7] in Mb forms a strong hydrogen bond with bound oxygen, and replacement with non-hydrogen-bonding amino acids greatly decreases O$_2$ affinity. In contrast, homologous His[E7] substitutions in Lba have very little effect on ligand affinity. Comparison of rate constants for ligand binding to wild type and distal pocket mutants of soybean Lba suggests that the unusual combination of His[E7] and Tyr[B10] works together to prevent His[E7] from forming a strong hydrogen bond with bound O$_2$ (*5*). To test this hypothesis, we have used FTIR spectroscopy to examine electrostatic fields and hydrogen-bonding interactions in the vicinity of bound CO for a complete set of Lba and Mb distal pocket mutants.

The IR spectrum of bound CO is a sensitive measurement of hydrogen-bonding and electrostatic interactions near the ligand (*16−24*). In native mammalian MbCO, the C−O

* Author to whom correspondence should be addressed [telephone (515) 294-2616; fax (515) 294-0453; e-mail msh@iastate.edu].
[‡] Iowa State University.
[§] Rice University.
[⊥] U.S. Department of Agriculture and University of Nebraska.

[1] Abbreviations: FTIR, Fourier transform infrared resonance; ν_{CO}, C−O stretching frequency; Lba, soybean leghemoglobin a; Mb, myoglobin; rice nsHb, rice nonsymbiotic hemoglobin I; lupin Lb, yellow lupine leghemoglobin I; cowpea Lb, cowpea leghemoglobin II; Hb, hemoglobin; IPTG, isopropyl-β-D-thiogalactoside; CO, carbon monoxide.
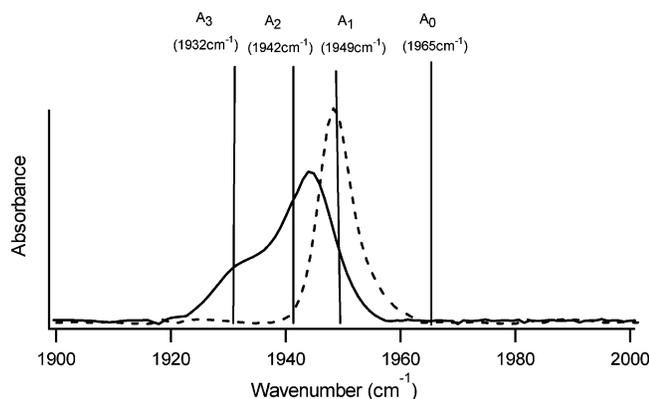
FIGURE 1: Comparison of the IR spectra of wild-type sperm whale MbCO and soybean LbaCO. The spectrum of MbCO (solid line) contains two major ν_{CO} peaks, one at 1945 cm^{-1}, representing a combination of the A_1 and A_2 conformers, and another at 1932 cm^{-1}, representing the A_3 conformer with a stronger hydrogen bond between His^{E7} and bound CO. LbaCO (broken line) exists as a single conformer with a peak at 1948 cm^{-1}.

stretching frequency (ν_{CO}) senses the proximity of the distal His and whether the Nϵ−H tautomer is donating a proton to the carbonyl O atom. The CO complexes of many Hbs and Mbs display multiple stretching frequencies between 1900 and 2000 cm^{-1}, with the major ν_{CO} peaks designated ν_0, ν_1, ν_2, etc., in the descending order of their frequencies (*19*). The structural origins of these multiple conformational substates have been studied in great detail for sperm whale MbCO. The designations A_0, A_{1-2}, A_3 (Figure 1) represent discrete conformations of ground-state native MbCO with ν_{CO} peaks at 1965, 1945, and 1932 cm^{-1}, respectively, based on low-temperature time-resolved IR experiments by Frauenfelder's group and deconvolution analyses of room temperature IR spectra by Caughey and co-workers (*18*, *19*, *23*, *25−28*).

Li and Spiro (*29*) interpreted the various ν_{CO} bands in terms of different extents of back-bond donation from the iron atom. They suggested that proton donors adjacent to the O atom of the bound ligand enhance the degree of back-bonding, increasing the order of the Fe−C bond and decreasing the order of the C−O bond due to the formation of Fe$^{\delta(+)}$=C=O$^{\delta(-)}$ resonance structures. The loss of hydrogen bonding or the presence of a negative electrostatic potential would reverse these effects. Oldfield et al. proposed short-range electric field-induced ν_{CO} frequency shifts due to 180° ring flips of the tautomers of the distal His and its movement away from the bound ligand at low pH (*30*, *31*). It was assumed that the distal His dominates the interaction with the bound ligand due to its proximity to CO and that enhancement, weakening, or loss of interaction with this residue accounted for all four conformers of MbCO.

More recently, Phillips, Olson, Franzen, and co-workers considered longer range interactions from internal fields arising from a sum of smaller interactions at a distance, as well as specific short-range hydrogen-bonding interactions with His^{E7} and other adjacent amino acid side chains (*19*, *32*). They concluded that, if the proximal geometry remains invariant, ν_{CO} is a reflection of the electrostatic fields and hydrogen-bonding interactions exerted by amino acid side chains close to bound CO and by itself does not unambiguously define a conformational substate (*18*, *19*, *33*). A positive potential or strong hydrogen bond donation lowers

ν_{CO}, whereas a negative potential or loss of hydrogen bonding increases ν_{CO}. Phillips et al. (*19*) also showed that there is a strong correlation between the average peak value, $\bar{\nu}_{CO}$, and the logarithm of the rate constant for O_2 dissociation, k_{O2}, for a series of 20 different Mbs. Thus, in Mb both $\bar{\nu}_{CO}$ and k_{O2} reflect the strength of hydrogen-bonding interactions between distal pocket amino acids and bound ligands.

In sperm whale MbCO, the principal CO stretching bands are $\nu_0 = 1965$ cm^{-1}, $\nu_1 = 1949$ cm^{-1}, $\nu_2 = 1942$ cm^{-1}, and $\nu_3 = 1932$ cm^{-1}, which have been assigned to the A_0, A_1, A_2, and A_3 conformational substates of the His^{E7} side chain (Figure 1; *16*, *21*, *22*, *25*, *26*, *34*, *35*). At neutral pH, the dominant band is at 1945 cm^{-1} and represents an average peak position for the A_1 and A_2 conformers, often simply called A_1. A minor A_3 substate is observed at $\nu_{CO} \approx 1932$ cm^{-1} (*18*). At low pH, the distal His swings out into the solvent, creating an apolar active site with $\nu_{CO} = \sim1960$ cm^{-1}. This Mb conformer is designated the A_0 substate.

In contrast, Lba shows a narrow CO stretching frequency band at 1948 cm^{-1}, indicating a single well-defined conformation at neutral pH (Figure 1) (*36*). This result suggests that the distal His in LbaCO is more restricted under physiological conditions than in sperm whale Mb, which exhibits significant conformational heterogeneity. In a series of high-resolution NMR studies, Mabbutt et al. (*37*, *38*) observed that the imidazole ring of His^{E7} in LbaCO appears to be "flipped" with respect to the orientation in sperm whale MbCO by a 180° rotation about the Cβ−Cγ bond. As a result, Nδ points upward, away from the heme plane and toward the protein interior, but Nϵ is still close to the bound ligand. The Nϵ−H tautomer of His^{E7} must still be dominant because the ν_{CO} peak of LbaCO (1948 cm^{-1}) is similar in position to $\bar{\nu}_{CO}$ for MbCO (1941 cm^{-1}), even though the 7 cm^{-1} shift to higher frequency does indicate a weaker hydrogen-bonding interaction in the plant protein.

Regulation of the position of His^{E7} and its hydrogen-bonding potential has been suggested as a possible mechanism for attenuating ligand affinity in Lba (*5*). As described above, FTIR spectroscopy is an ideal tool for assessing the effects of distal pocket mutations on the electrostatic and/or hydrogen-bonding environment of bound CO and for testing structural mechanisms for regulation of ligand binding. In the present study, CO stretching frequencies for a comprehensive set of distal pocket mutants of Lba have been measured. The results have been compared to IR spectra of equivalent mutants of sperm whale Mb. In both proteins, Tyr^{B10} appears to inhibit hydrogen-bonding interactions between His^{E7} and bound CO and O_2 (*5*, *13*). The new IR and previous O_2 binding and NMR results suggest that there is a direct interaction between the His^{E7} and Tyr^{B10} side chains in Lba that weakens stabilization of bound ligands.

MATERIALS AND METHODS

Preparation, Expression, and Purification of Proteins. Site-directed mutant cDNAs were constructed, and recombinant Mbs and Lbs were expressed and purified as described previously (*4−6*, *18*). Mutations were introduced at the key helix positions E7, E11, and B10 (Figure 2). Yellow lupine leghemoglobin I (lupin Lb) cDNA in pET 3a was provided by Dr. Pawel M. Strozycki, Institute of Bioorganic Chemistry, Polish Academy of Sciences, Poland. The lupin Lb
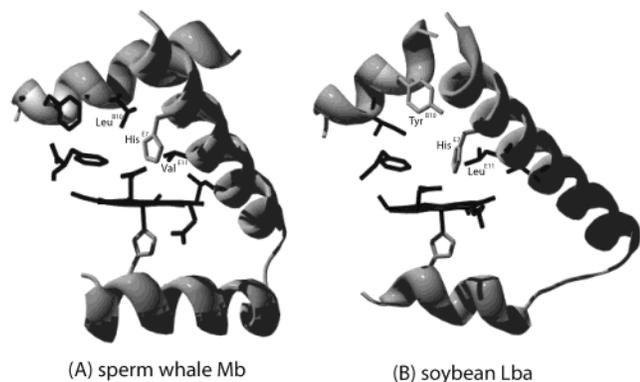
FIGURE 2: Amino acid side chains in the heme pockets of (A) sperm whale Mb and (B) soybean Lba. The polar side chains are in gray and the apolar ones in black. The key amino acids (B10, E7, and E11) are labeled. His^{E7}, the seventh residue on the E helix and 64th residue on the polypeptide chain, is the only polar side chain in Mb close enough to directly interact with the bound ligand. In Lba, however, both His^{E7} (61st residue) and Tyr^{B10} (30th residue) are polar, but only His^{E7} is close enough to the iron to interact directly with diatomic ligands. The Mb and Lba structures were taken from Quillin et al. (47) [Protein Data Bank (PDB) 2MBW] and Hargrove et al. (4) (PDB 1BIN), respectively.

cDNA was subcloned into Novagen expression vector pET 29a between *Nde*I and *Eco*RI restriction sites and expressed in *Escherichia coli* BL21(λDE3)-CodonPlus-RP cells (Stratagene) grown in 2× YT medium at 37 °C. The medium in shake flasks was supplemented with 50 μg/mL kanamycin and 25 μg/mL chloramphenicol. Approximately 6.5 h after inoculation, expression was induced with 0.5 mM IPTG. After induction, the growth was continued for a further 15 h, resulting in red cell pellet. The lupin LbI protein was purified in the same way as soybean Lba (6). Cowpea leghemoglobin II (cowpea Lb) was purified according to methods described previously (39). All samples were oxidized and stored in the ferric form.

FTIR Spectroscopy and Kinetic Measurements. Samples of CO-bound and deoxygenated Lba and Mb were prepared in stoppered Eppendorf tubes equilibrated with 1 atm of either CO or N_2. Approximately 20 μL of 2−3 mM protein was aliquoted into this tube with a syringe. The Eppendorf tube was then re-equilibrated with either pure CO or N_2 gas. One microliter of a 200 mM dithionite solution in 100 mM phosphate buffer, pH 7.0, was added to the tube to reduce any oxidized iron and to remove molecular oxygen. The tube was vortexed and then spun in a microcentrifuge to remove any precipitate. An airtight syringe, equilibrated with nitrogen gas, was then used to draw LbaCO or deoxyLba from the tube. The protein sample was rapidly added to a CaF_2 BioCell IR cuvette (5 mm thickness × 50 mm diameter, separated by a 40 μm spacer; BioTools, Inc.) to obtain a uniform, bubble-free film. Then the windows of the cuvette were quickly sealed. The cuvette was placed in the sample chamber of a Nicolet Nexus 470 FTIR spectrometer (Nicolet Instrument Corp., Middleton, WI), which was purged with nitrogen gas 1 h prior to and then during data collection. Spectra were recorded from 1800 to 2100 cm^{-1} at 1 cm^{-1} resolution. Up to 128 interferograms were averaged for both the HbCO and deoxyHb control samples. The final FeCO FTIR spectra were corrected for buffer and protein background by computing LbaCO minus deoxyLba difference spectra.
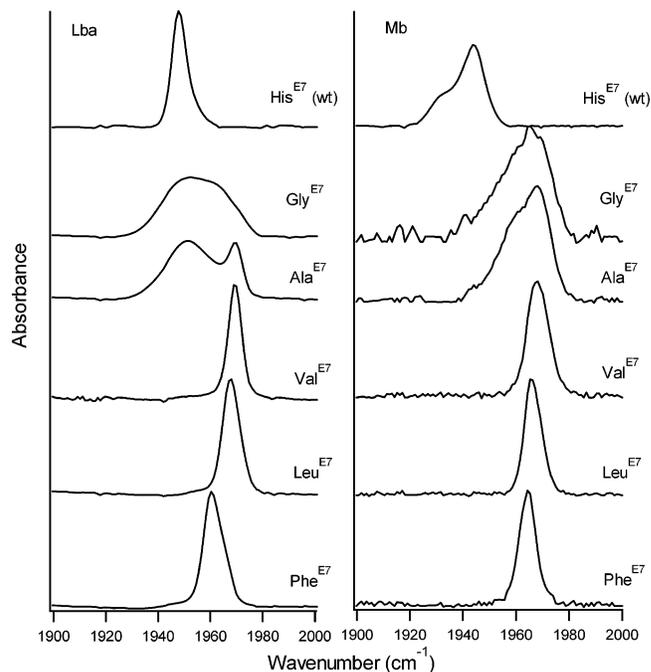

FIGURE 3: IR spectra of LbaCO and MbCO mutants with apolar substitutions at position E7. The mutants are designated by a three-letter abbreviation for the substituted amino acid with a superscript denoting the position on the E helix. All of the spectra for the E7 Mb mutants are shifted to higher frequencies due to the loss of hydrogen-bonding interactions with His^{E7}. The E7 Lba mutants show similar shifts to higher stretching frequencies. However, the Lba mutants with smaller amino acids at E7 show retention and broadening of the peak at ∼1950 cm^{-1}, presumably due to interactions with water molecules entering the "empty" distal pocket. The spectra for the MbCO mutants were taken from Li et al. (18).

Most of the rate constants for CO and O_2 binding were measured previously (see references in Tables 1−3). The parameters for any new mutants were determined as described in Kundu et al. (5) and Rohlfs et al. (40).

Computations and Molecular Modeling. Tyr^{B10} and His^{E7} rotomers in the Lba−acetate structure (PDB 1BIN) were suitably oriented in the program O (41) to incorporate the imidazole conformation proposed by Mabbutt et al. (37, 38) and to model possible interactions between Tyr^{B10} and His^{E7}. NMR chemical shifts for the protons in Tyr^{B10} and His^{E7} side chains were predicted for the proposed model structures using the program SHIFTS (42).

RESULTS

His^{E7} Hydrogen Bonds to Bound CO Less Strongly in Lba than in Mb. CO bound to heme within a nonpolar distal pocket typically yields a single IR peak near 1965 cm^{-1} and is shifted to an average value of 1941 cm^{-1} in wild-type Mb (Figure 3; Table 1) (18). This blue shift is due to the positive electrostatic field created at the ligand by a hydrogen bond donated from the distal His (18−20). The absorption at 1948 cm^{-1} by wild-type LbaCO also implies a hydrogen bond to the bound ligand, although a weaker one compared to Mb. In Lba, His^{E7} and Tyr^{B10} could potentially serve as proton donors (Figure 2).

The Phe^{E7}, Leu^{E7}, and Val^{E7} mutants of Lba show single bands at 1960, 1968, and 1969 cm^{-1}, respectively, indicating the loss of a hydrogen bond from the distal His (Figure 3;

Table 1: IR CO Stretching Bands for Soybean Lba, Sperm Whale Mb,[a] and Their Mutant Proteins at pH 7 and 25 °C

protein	$\nu_0{}^b$ (%) (cm^{-1})	$\nu_{1,2}$ (%) (cm^{-1})	ν_3 (%) (cm^{-1})	$\nu_{CO}{}^c$ (cm^{-1})	protein	ν_0 (%) (cm^{-1})	$\nu_{1,2}$ (%) (cm^{-1})	ν_3 (%) (cm^{-1})	ν_{CO} (cm^{-1})
wild-type Lba[d]		1948 (100)		1948	wild-type Mb	1945[e] (70)	1932[e] (30)		1941[e]
His61 (E7) mutants					His64 (E7) mutants				
Gly^{E7}	1961 (48)	1952 (52)		1956	Gly^{E7}	1965 (100)			1965
Ala^{E7}	1969 (49)	1951 (51)		1959	Ala^{E7}	1966 (100)			1966
Val^{E7}	1969 (100)			1969	Val^{E7}	1967 (100)			1967
Leu^{E7}	1968 (100)			1968	Leu^{E7}	1965 (100)			1965
Phe^{E7}	1960 (100)			1960	Phe^{E7}	1964 (100)			1964
Trp^{E7}	1959 (38)	1940 (62)		1947	Trp^{E7}	1969 (60)	1942 (40)		1958
Tyr^{E7}	1968 (55)	1953 (45)		1961	Tyr^{E7}	1966 (100)			1966
Gln^{E7}	1957 (63)	1943 (37)		1952	Gln^{E7}		1945 (100)		1945
Lys^{E7}	1968 (42)	1959 (58)		1962	Lys^{E7}	1965[e] (56)	1956[e] (44)		1961[e]
Arg^{E7}	1957 (30)	1944 (34)	1940 (36)	1946	Arg^{E7}	1958[e] (100)			1958[e]
Leu65 (E11) mutants					Val68 (E11) mutants				
Val^{E11}		1948 (100)		1948	Leu^{E11}		1941 (75)	1930 (25)	1938
Phe^{E11}		1948 (100)		1948	Phe^{E11}		1945 (64)	1932 (36)	1940
Tyr30 (B10) mutants					Leu29 (B10) mutants				
Gly^{B10}	1966 (39)	1949 (26)	1927 (35)	1948	Gly^{B10}	f	f	f	f
Ala^{B10}	1963 (29)	1949 (34)	1926 (37)	1944	Ala^{B10}	1965 (6)	1947 (51)	1935 (43)	1943
Val^{B10}	1967 (3)	1950 (41)	1927 (56)	1938	Val^{B10}	1965 (6)	1946 (43)	1933 (51)	1941
Leu^{B10}	1973 (5)	1951 (30)	1928 (65)	1937	Ile^{B10}	1965 (4)	1945 (48)	1932 (48)	1940
Phe^{B10}	1960 (13)	1951 (44)	1923 (43)	1940	Phe^{B10}			1932 (100)	1932
Trp^{B10}	1961 (52)	1948 (39)	1925 (9)	1953	Trp^{B10}	1956 (37)	1945 (63)		1949
Arg^{B10}	1965 (75)	1948 (17)	1929 (8)	1958	Arg^{B10}	f	f		f
					Tyr^{B10}	1981[e] (31)	1969[e] (39)	1931[e] (30)	1961[e]
double mutant					double mutants				
Leu^{B10}Ala^{E7}	1965 (100)			1965	Tyr^{B10}Gln^{E7}			1934[e] (100)	1934[e]
					Tyr^{B10}Leu^{E7}	1968[e] (14)		1936[e] (86)	1940[e]

[a] Data taken from Li et al. (18) unless mentioned otherwise. [b] The frequency of the IR band was determined by the peak position, with estimated experimental error ±1 cm^{-1}; the intensity of the IR band was determined by the peak height and was normalized to the strongest band with estimated experimental error ±10%. [c] The value of ν_{CO} is a weighted measurement of the IR CO spectral components, as computed by $\nu_{CO} = \Sigma f_i \nu_i$, where f_i is the fraction of intensity measured by peak height and ν_i is the peak frequency of spectral component i. [d] Four conformers were tentatively assumed in Lba for comparison with Mb. [e] Measured by the authors. [f] Data not available.

Table 1). These peaks are similar to those observed for CO—heme complexes within a completely apolar binding pocket and imply that Tyr^{B10} makes no significant direct contribution to the electrostatic environment of the bound ligand. In the wild-type metLba structure (4), the Tyr^{B10} side chain is too far away from the iron atom to hydrogen bond directly with bound ligands without significant movements of the B and E helices (Figure 2). This conclusion is supported by the close similarity of the ν_{CO} bands observed for the Phe^{E7}, Leu^{E7}, and Val^{E7} mutants, which contain Tyr^{B10}, and the ν_{CO} band at 1965 cm^{-1} seen in the completely apolar Leu^{B10}-Ala^{E7} double mutant of Lba (Figure 4; Table 1). Conversely, Leu^{B10} (which still contains His^{E7}) shows an IR band at much lower frequency, indicating that a strong hydrogen bond can be formed between bound CO and the distal His in the absence of the Tyr side chain (Figure 4).

Water molecules in the exposed distal pockets of Gly^{E7} and Ala^{E7} MbCO broaden the observed ν_{CO} peaks (18, 19), and a similar explanation probably accounts for the heterogeneity observed in the IR spectra of Gly^{E7} and Ala^{E7} LbaCO (Figure 3). The spectrum of Gly^{E7} LbaCO is unusually broad, with two obvious shoulders at 1952 and 1961 cm^{-1} (Table 1). The Ala^{E7} LbaCO spectrum has two distinct peaks. The narrow band at 1969 cm^{-1} indicates a conformation with a completely apolar environment near bound CO. The broad band centered at ~1951 cm^{-1} (similar to that seen in Gly^{E7}) indicates favorable hydrogen-bonding interactions, presumably with distal pocket water molecules. This interpretation is supported by the IR spectrum of the Leu^{B10}Ala^{E7} LbaCO double mutant, which has no polar residues or stabilized water molecules and shows a single narrow band centered at ν_{CO} = 1965 cm^{-1} (Figure 4; Table 1). The lack of any
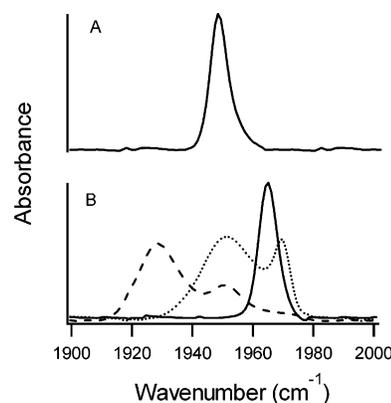

FIGURE 4: Comparison of the IR spectra of (A) wild-type LbaCO and (B) B10/E7 mutants of LbaCO. When Tyr^{B10} is replaced with Leu (Leu^{B10}, - - -), a major band at a very low frequency is observed. Ala^{E7} LbaCO (···) shows a broad band at the "normal" frequency and another narrow band at high frequency. In contrast, the double mutant (Leu^{B10}Ala^{E7}, —), from which both of the polar side chains have been removed, shows only a single narrow band at high frequency (Table 1).

hydrogen-bonding interactions in the double mutant is also apparent from its much larger rate constant for O$_2$ dissociation ($k_{O2} \approx 100$ s^{-1}) compared to those for wild-type LbaO$_2$ ($k_{O2} \approx 6$ s^{-1}) and the two corresponding single mutants ($k_{O2} \approx 1{-}3$ s^{-1}) (Table 2). Thus, although His^{E7} is the main source of polarity around bound ligands in Lba, hydrogen bonding is relatively weak, and Tyr^{B10} can have a significant indirect influence. This results in differences in the electrostatic interactions with bound ligands in the distal heme pockets of Lba and Mb.

Table 2: Correlations between IR CO Stretching Bands and Ligand Binding Parameters for Lba and Sperm Whale Mb[a] at pH 7 and 25 °C

protein	ν_{CO} (cm⁻¹)	k_{CO} (s⁻¹)	K_{CO} (μM⁻¹)	k_{O_2} (s⁻¹)	K_{O_2} (μM⁻¹)	protein	ν_{CO} (cm⁻¹)	k_{CO} (s⁻¹)	K_{CO} (μM⁻¹)	k_{O_2} (s⁻¹)	K_{O_2} (μM⁻¹)
wild-type Lba	1948	0.0084	1800	5.6	23	wild-type Mb	1941	0.019	27	15	1.1
His61 (E7) mutants						His64 (E7) mutants					
Gly[E7]	1956	0.0066	15000	3.6	97	Gly[E7]	1965	0.038	150	1600	0.09
Ala[E7]	1959	0.0061	14000	3.1	93	Ala[E7]	1966	0.061	69	2300	0.025
Val[E7]	1969	0.0016	75000	27	10	Val[E7]	1967	0.048	150	10000	0.011
Leu[E7]	1968	0.0024	70000	24	17	Leu[E7]	1965	0.024	1100	4100	0.023
Phe[E7]	1960	0.013	1800	280	0.45	Phe[E7]	1964	0.054	83	10000	0.0074
Tyr[E7]	1961	0.011	130	3.1	1.3	Tyr[E7]	1966	0.092	5.4	3200	0.0021
Trp[E7]	1947	0.0098	3	7.8	0.04	Trp[E7]	1958	0.023	28	87	0.071
Gln[E7]	1952	0.0094	7500	3.6	72	Gln[E7]	1945	0.012	82	130	0.18
Lys[E7]	1962	0.0048	13000	2.9	100	Lys[E7]	1961	0.038	195	760	0.12
Arg[E7]	1946	0.006	13000	0.2	1200	Arg[E7]	1958	0.014	400	880	0.09
Leu65 (E11) mutants						Val68 (E11) mutants					
Val[E11]	1948	0.0069	2000	5.8	30	Leu[E11]	1938	0.011	48	6.8	3.4
Phe[E11]	1948	0.0036	8300	1.8	105	Phe[E11]	1940	0.018	14	2.5	0.48
Tyr30 (B10) mutants						Leu29 (B10) mutants					
Gly[B10]	1948	0.0054	1300	0.8	75						
Ala[B10]	1944	0.011	1200	0.9	84	Ala[B10]	1943	0.019	14	18	0.8
Val[B10]	1938	0.006	1800	0.3	80	Val[B10]	1941	0.016	11	8.3	1.1
Leu[B10]	1937	0.0054	2000	0.5	74	Ile[B10]	1940	0.018	13	10	0.86
Phe[B10]	1940	0.0068	1600	0.75	100	Phe[B10]	1932	0.006	37	1.4	15
Trp[B10]	1953	0.0073	9600	1.1	175	Trp[B10]	1949	0.008	0.48	8.5	0.029
Arg[B10]	1958	0.0091	1100	1.3	35	Tyr[B10]	1961	0.11[b]	~3.0[b]	20000[b]	~0.001[b]
								~0.004[b]		200[b]	~0.010[b]
								−0.01		20[b]	
double mutant						double mutants					
Leu[B10]Ala[E7]	1965	0.0028	58000	96	6	Tyr[B10]Leu[E7]	1940	0.011[c]	91[c]	14[c]	1.6[c]
						Tyr[B10]Gln[E7]	1934	0.014[b]	5.1[b]	1.6[b]	1.8[b]

[a] Data taken from Li et al. (*18*) and Kundu et al. (*5*). [b] Data from Draghi et al. (*13*). [c] Measured by the authors.

Role of the B10 Side Chain in Positioning His[E7] in Mb and Lba. An important difference between Lba and Mb is the Tyr found at the B10 helical position in the former instead of an apolar Leu in the latter (Figure 2). Replacement of Tyr[B10] in LbaCO by any other amino acid, irrespective of size or polarity, results in the appearance of multiple ν_{CO} peaks (Figure 5; Table 1). In general, the IR spectra of the B10 mutants are mixtures of high- and low-frequency bands, which are completely absent in wild-type LbaCO. The low-frequency ν_{CO} peaks for the B10 LbaCO mutants are at ~1926 cm⁻¹, which is significantly lower than those seen in the B10 mutants of sperm whale MbCO (~1932 cm⁻¹, Figure 5; Table 1). The low-frequency peaks in the Lba B10 mutants must be due to conformations in which the distal His forms a much stronger hydrogen bond with bound CO than that in the native protein. This interpretation in terms of more favorable electrostatic interactions is supported by the uniform decrease in the rate constant for O_2 dissociation from all of the B10 mutants compared to wild-type LbaO₂ (Table 2).

The average ν_{CO} for the apolar B10 LbaCO mutants is lower than that of wild-type LbaCO (Table 1). However, there are also bands in the 1960−1970 cm⁻¹ range, indicating conformations with completely apolar binding sites and no interaction with the distal His. Thus, when Tyr[B10] in Lba is replaced by other amino acids, the side chain of His[E7] adopts multiple orientations, some of which involve formation of strong hydrogen bonds with bound ligands and some of which involve no interaction at all. In contrast, apolar B10 mutations in Mb only enhance the low-frequency band associated with the A₃ conformer ($\nu_{CO} \approx 1932$ cm⁻¹). Little or no intensity associated with high-frequency bands at ν_{CO} = 1960−1970 cm⁻¹ is seen (Figure 5; Table 1). The IR spectrum of Phe[B10] MbCO has a single band at 1932 cm⁻¹. The crystal structures of Phe[B10] MbCO and MbO₂ show that His[E7] is fixed in a more A₃-like conformation and the positive edge of the benzyl side chain points toward the bound ligand (*18*). This conformation causes a ~10-fold decrease in the rate of O_2 dissociation from Phe[B10] MbO₂ compared to that from the wild-type protein (Table 2; *43*).

The Trp[B10] mutations in both LbaCO and MbCO cause a shift in $\bar{\nu}_{C-O}$ to higher frequencies, and there is minimal appearance of strong low-frequency bands in the 1920−1935 cm⁻¹ region (Table 1). In these cases, the large size of the indole ring appears to be "pushing" the distal His away from bound ligands. The Arg[B10] mutation in LbaCO causes a more significant effect, increasing $\bar{\nu}_{C-O}$ from 1948 to 1958 cm⁻¹, suggesting that the His[E7] side chain has been pushed out into the solvent. Because the B10 side chain in Lba is too far from the active site, the guanidino group of Arg[B10] cannot access the bound ligands either to interact favorably with them (Figure 2).

The Tyr[B10] mutation produces the largest effect on the IR spectrum of MbCO, causing the appearance of multiple bands from 1931 to 1980 cm⁻¹ (Figure 5). Thus, a Tyr side chain at the B10 position in Mb has the opposite effect of that observed in Lba. The phenolic side chain in Mb causes multiple conformations with positive and negative fields adjacent to the bound ligand. This interpretation is supported by the multiple phases seen for O_2 dissociation from Tyr[B10] MbO₂ (*13*; Table 2). In contrast, the Tyr[B10] side chain in native Lba "traps" His[E7] in a single conformational state, which can only donate a weak hydrogen bond to bound ligands. When Tyr[B10] is replaced by Leu in LbaCO (a distal pocket akin to Mb), His[E7] is able to adopt a conformation with a much stronger hydrogen bond to bound ligands as
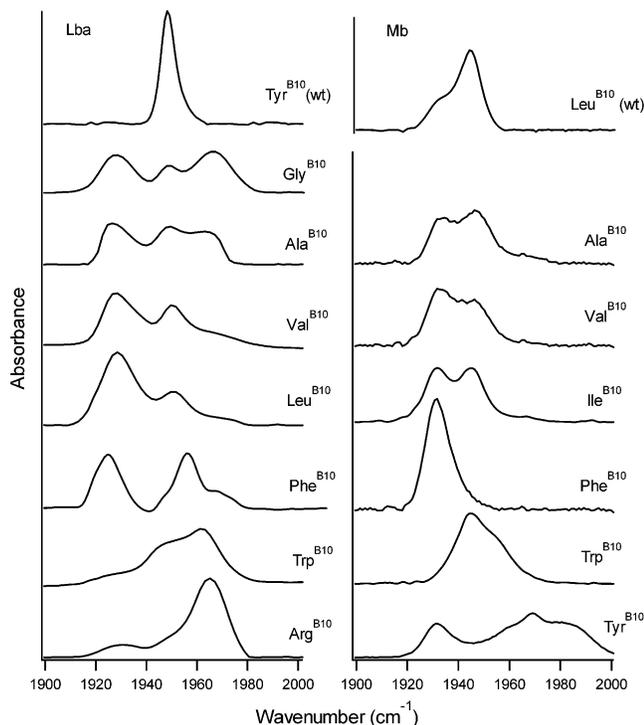
FIGURE 5: IR spectra of B10 mutants of soybean LbaCO and sperm whale MbCO. All of the Lba mutants show multiple peaks, including at least one low-frequency band. Most of the B10 mutations in Mb change only in the proportion of the ν_1 versus ν_3 bands, with Phe^{B10} MbCO showing only a single conformer at ν_3 = 1932 cm^{-1}. In contrast, the Tyr^{B10} mutation in MbCO causes the appearance of a major high-frequency band at 1969 cm^{-1}. The spectra for the Ala, Val, Ile, and Phe B10 Mb mutant proteins were taken from Li et al. (*18*); the other spectra were measured in this work.

seen by the appearance of a major ν_{CO} band at 1926 cm^{-1} (Figure 5). This conclusion is supported by the 10-fold drop in the rate of O$_2$ dissociation from the same Lba mutant (Table 2).

Polar Mutations at the E7 Position. As shown in Figure 6, the native Tyr^{B10} side chain in Lba also affects the position of polar amino acids when they are inserted into the E7 helical position as compared to their positions in analogous E7 mutants of Mb. The most dramatic differences between the two proteins are observed for the single Arg^{E7} mutants. In Arg^{E7} MbCO, a single, narrow high-frequency band at 1958 cm^{-1} is observed (Figure 6) and has been interpreted in terms of the Arg^{E7} guanidino group pointing into the solvent, as has been observed in Hb Zurich (β His^{E7}→Arg) (*44−47*). In contrast, several bands are observed for Arg^{E7} LbaCO (Table 1). The majority of the conformers occur at relatively low frequencies in the 1940−1945 cm^{-1} region (Figure 6), indicating a positive electrostatic field adjacent to bound CO. More remarkably, the His^{E7}→Arg mutation in Lba causes the rate constant for O$_2$ dissociation to decrease by ~30-fold, indicating that an even stronger stabilizing interaction occurs when dioxygen is bound (Table 2). In contrast, the His^{E7}→Arg mutation in Mb causes k_{O2} to increase from 15 to ~1000 s^{-1}, indicating the loss of stabilizing electrostatic or hydrogen-bonding interactions.

Taken together, these spectroscopic and ligand-binding data suggest that the guanidino group of Arg^{E7} can remain in the distal pocket of Lba. In the CO complex, the side chain adopts multiple conformations. The guanidino group
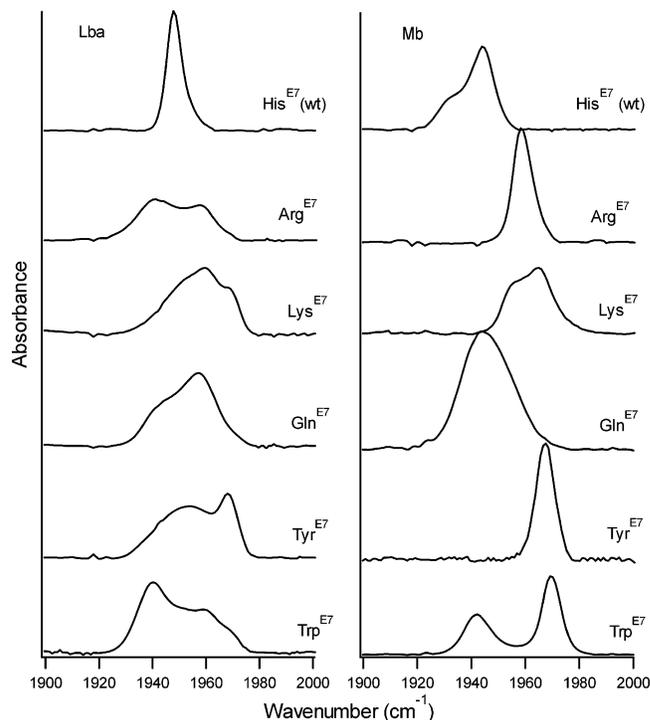
FIGURE 6: IR spectra of LbaCO and MbCO mutants with charged or polar residues at position E7. Arg^{E7} MbCO shows a single, high-frequency peak indicating that this residue does not interact with bound CO. In contrast, Arg^{E7} LbaCO shows multiple bands with significant populations of conformers having lower ν_{CO}, suggesting that this side chain can form hydrogen bonds with bound CO. The Lys^{E7} mutants for both, however, are predominantly in conformations with higher ν_{CO} and possibly have their side chains swinging out of the distal heme pocket. Gln^{E7} MbCO and LbaCO show peak positions similar to those of the wild-type proteins, but the bands are broader. Tyr^{E7} in MbCO exclusively provides an apolar environment to bound CO, whereas Tyr^{E7} in LbaCO provides some positive potential as well. Trp^{E7} MbCO and LbaCO show a conformer with lower ν_{CO} in addition to a higher one. The spectra for Arg^{E7} and Lys^{E7} MbCO mutant proteins were measured for this work, and the others were taken from Li et al. (*18*).

can either swing out into solvent, causing an apolar active site and an increase in ν_{CO}, or remain in the pocket, causing an increase in the electrostatic field near the bound ligand and a decrease in ν_{CO}. The latter "in" conformation appears to be the dominant one when Arg^{E7} Lba binds O$_2$, as judged by the dramatic decrease in k_{O2} (Table 2). The Tyr^{B10} hydroxyl O atom probably helps to stabilize the "in" conformation by acting as a hydrogen bond acceptor for the guanidino group, and the partial negative charge on bound O$_2$ provides additional electrostatic stabilization. In Mb, the naturally occurring Leu^{B10} side chain cannot facilitate internalization of the Arg^{E7} side chain, and the free energy released by solvation of the guandino group out-competes any weak, favorable interaction with bound ligands. In addition, the size of the distal pocket in Mb is smaller and probably cannot easily accommodate the large Arg^{E7} side chain.

The effects of the His^{E7}→Lys^{E7} mutation on the IR spectra of MbCO and LbaCO are much more similar than in the case of the Arg^{E7} replacement (Figure 6). In both proteins, most of the absorbance occurs at higher frequencies, indicating that the dominant conformations have the primary amine pointing out of the pocket, increasing the apolar character of the ligand binding site. The Gln^{E7} mutations in both proteins cause little change in the average ν_{CO} value but do
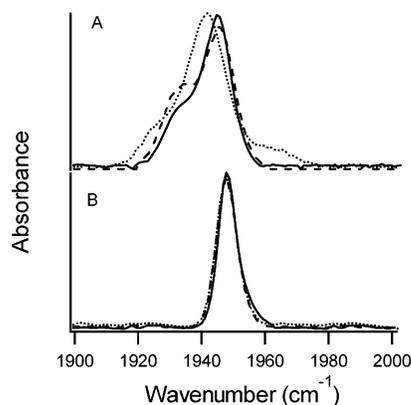
FIGURE 7: IR spectra of position E11 mutants of (A) sperm whale MbCO and (B) soybean LbaCO. Spectra for the wild-type proteins are shown as solid lines. When Val^{E11} is replaced with Leu (···) or Phe (- - -) in Mb, the resulting IR spectra of mutant proteins are different from the wild-type MbCO spectrum. When Leu^{E11} in LbaCO is replaced with Val (···) and Phe (- - -), there is no change in the measured IR spectrum. The spectra for the MbCO mutants were taken from Li et al. (*18*).

broaden the major bands, presumably due to the flexible nature of the amide side chain and the potential for electrostatic interactions with either the carbonyl O atom or the amide protons.

The Tyr^{E7} substitutions cause shifts to higher frequencies in both proteins, suggesting that either the phenolic side chain moves out of the active site or that the nonbonded electrons of the phenoxyl O atom are pointed toward the bound ligand. In MbCO, the former interpretation probably applies because a single, narrow band is observed at 1966 cm^{-1}. In LbaCO, a narrow band is observed at 1968 cm^{-1}, but a large, broad band also occurs around 1950 cm^{-1} and is similar to that seen for the Ala^{E7} LbaCO complex. The Trp^{E7} mutant proteins of Lba and Mb show two principal conformers. The dominant conformer in LbaCO has a low-frequency band at $\nu_{CO} = 1939$ cm^{-1}, whereas the dominant conformer in MbCO has a high-frequency band at 1969 cm^{-1} (Figure 6; Table 1). The indole N−H group or the positive edge of the aromatic multipole of Trp^{E7} probably interacts with bound CO in the low-frequency conformers of both proteins, resulting in the appearance of bands in the 1940 cm^{-1} region (*18*).

Leu^{E11} in Lba Has Little Effect on Hydrogen Bonding. Val^{E11} in Mb is important for maintaining the appropriate distal pocket volume for ligand binding and prevention of autoxidation (*47*), and mutations at this position have been found to influence the MbCO IR spectra significantly (*18, 19, 47−49*). As seen in Figure 7A and Table 1, even relatively subtle mutations at the E11 position in Mb affect its IR spectrum. However, the corresponding Lba mutant proteins leave the IR spectra completely unaltered (Figure 7B). Apolar replacement of Leu^{E11} in Lba also has only small, subtle effects on protein stability and ligand-binding kinetics (*5*). The crystal structure of Lba shows that the naturally occurring Leu^{E11} side chain is behind the distal His, almost on the far interior side of the ligand-binding site compared to the position of Val^{E11} in Mb (*4*). Therefore, the importance of this amino acid in Mb is not shared in the distal pocket of Lba.

Role of the B10 Amino Acid in Other Leghemoglobins. Tyr is not conserved at position B10 in all leghemoglobins.
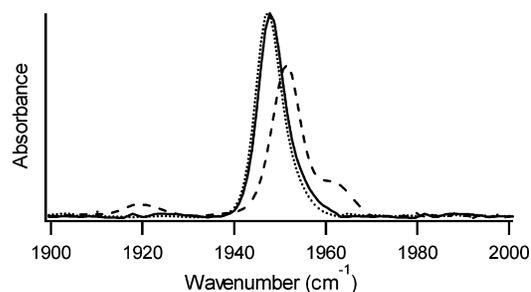

FIGURE 8: IR spectra of the CO complexes of leghemoglobins from different species of plants. Both cowpea (···) and soybean (−) Lb have a His^{E7}−Tyr^{B10} distal pair and identical IR spectra. Lupin (- - -) Lb has a His^{E7}−Phe^{B10} distal pair and shows a different IR spectrum with additional minor low- and high-frequency peaks.

Table 3: IR CO Stretching Bands for Three Leghemoglobins at pH 7 and 25 °C

protein	$\nu_0{}^a$ (%) (cm^{-1})	$\nu_{1,2}$ (%) (cm^{-1})	ν_3 (%) (cm^{-1})	$\nu_{CO}{}^b$ (cm^{-1})	k_{CO} (s^{-1})	k_{O2} (s^{-1})
soybean Lba		1948 (100)		1948	0.0084	5.6
cowpea LbII		1947 (100)		1947	0.01^c	5.5^c
lupin LbI	1962 (18)	1951 (75)	1919 (7)	1951	0.014^c	20^c

^{a,b} See footnotes *b* and *c* of Table 1. ^{c} Data taken from Gibson et al. (*51*).

Other species, most notably lupin, contain Phe at this site (*50*). To examine the importance of this naturally occurring Tyr→Phe replacement, IR spectra for cowpea LbII (Tyr^{B10}) and lupin LbI (Phe^{B10}) were measured (Figure 8). Cowpea LbII has an IR spectrum identical to that of soybean Lba, with a single conformer at 1948 cm^{-1} (Table 3). Both of these Lbs have a distal His^{E7}−Tyr^{B10} pair, nearly identical rate constants for oxygen binding (Table 3) (*51*), and presumably similar mechanisms for regulating ligand binding.

As shown in Figure 5, replacing Tyr^{B10} with Phe causes profound changes in the IR spectrum of soybean LbaCO, leading to the appearance of a large low-frequency band centered at 1923 cm^{-1} and the retention of a peak at 1950 cm^{-1}. The IR spectrum of lupin LbICO is different from those of both native soybean Lba and its Phe^{B10} mutant. However, a major band (∼75%) is observed at 1951 cm^{-1}, which is similar in position to that for cowpea and soybean LbCO. Thus, in lupin LbICO there must be constraints other than Tyr^{B10} that position His^{E7} in a conformation that allows only weak hydrogen bonding to bound CO. Harutyunyan et al. (*52*) have suggested that the His^{E7} side chain in the lupin LbICO crystal structure appears to be fixed in position by a lattice of hydrogen bonds linking Nδ of the imidazole side chain to well-defined water molecules, Glu^{E3}, and one of the heme propionates. However, these constraints do not appear to be as strong as those imposed by Tyr^{B10} in the other Lbs, because lupin LbICO also shows minor low- (7%) and high-frequency (18%) bands at 1920 and 1962 cm^{-1}, respectively (Table 3).

The Tyr^{B10}−His^{E7} Combination Destabilizes Bound Ligands. The side chain at the B10 position in Mb is close enough to make direct contact with bound ligands. However, multiple ν_{CO} bands and heterogeneous ligand binding are observed for the single Tyr^{B10} Mb mutant, and there is a net increase in $\bar{\nu}_{CO}$ and the average value of k_{O2} (Table 2; Figure 9A). Draghi et al. (*13*) have proposed that Try^{B10} and His^{E7}
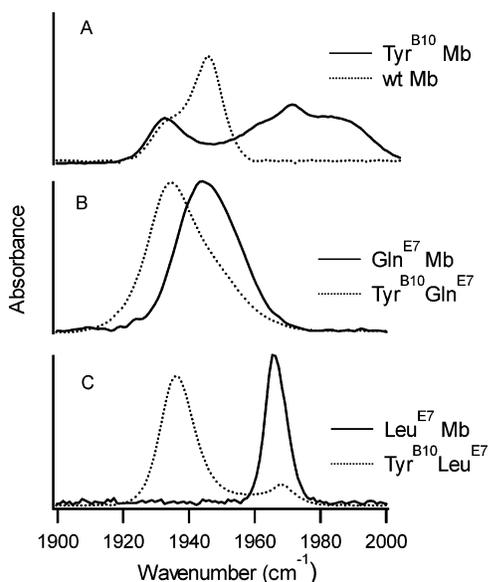
FIGURE 9: IR spectra of sperm whale MbCO mutants with Tyr at position B10. (A) IR spectra for wild-type MbCO (···) and for the Tyr^{B10} single mutant (—), which shows a major high-frequency band, suggesting that Tyr^{B10} prevents His^{E7} from stabilizing bound CO. In contrast, major low-frequency bands are observed for MbCO mutants containing the combination of (B) Tyr^{B10} and Gln^{E7} (···) or (C) Tyr^{B10} and Leu^{E7} (···). The corresponding single-mutants Gln^{E7} and Leu^{E7} show peaks at much higher frequencies. The results in panels B and C show that Tyr^{B10} can hydrogen bond directly to bound CO in the absence of His^{E7}.

sterically "clash" so that neither side chain can easily hydrogen bond to bound ligands. Replacement of the distal His with Gln allows the phenol side chain to interact favorably and directly with bound ligands in the Tyr^{B10}Gln^{E7} Mb double mutant (Figure 9B; Table 2; *13* and references therein). When His^{E7} is replaced with Leu in Tyr^{B10} MbCO, a major (86%) low-frequency band appears at 1936 cm^{-1} (Figure 9C), and the value of k_{O2} for the Tyr^{B10}Leu^{E7} double mutant is markedly decreased compared to the corresponding rate constants for the single E7 or B10 Mb mutants (Table 2; *13*). Thus, in the absence of a distal His, Tyr^{B10} can interact directly and favorably with bound ligands in mammalian Mbs.

A major conclusion from the IR and ligand-binding data in Table 2 is that the Tyr^{B10}–His^{E7} combination weakens hydrogen bonding to bound ligands in both Lba and Mb. In Mb, the two residues clash sterically, causing multiple conformations (IR bands) and kinetic phases (Figures 5 and 9; *13*). In Lba, the two residues appear to interact specifically forming a single conformation, as judged by the narrow symmetric CO IR band. As described below, the simplest explanation is that Tyr^{B10} "pulls" His^{E7} slightly away from the bound ligand by forming a hydrogen bond between the phenolic proton and the nonbonded electrons of the Nδ of His^{E7} (Figure 10A), an interpretation that is supported by modeling of the crystal structure of acetate–metLba (*4*) and by high-resolution NMR data (*37*, *38*, *53*).

DISCUSSION

Structural Model for His^{E7}–Tyr^{B10} Interactions in Lba. The experimental evidence in favor of a Tyr^{B10}–His^{E7} interaction in Lba is threefold. (1) Multiple ν_{CO} bands appear when Tyr^{B10} is replaced by almost any other amino acid. These

results suggest that in native Lba the phenol side chain holds His^{E7} in a fixed location farther away from bound ligands than the position of His^{E7} in Mb. In almost all of the Lba B10 mutants, a low-frequency band is observed at ~1925 cm^{-1}, indicating that a stronger hydrogen bond can form between His^{E7} and bound CO in the absence of Tyr^{B10}. (2) The B10 Lba mutations also cause significant decreases in k_{O2}, indicating a strengthening of the hydrogen bond to bound O$_2$ when His^{E7} is "freed" from its interaction with the phenol side chain of Tyr^{B10}. (3) Replacement of His^{E7} with large aliphatic residues (Val and Leu) causes a 20 cm^{-1} increase in the peak position of the major ν_{CO} band, indicating loss of hydrogen bonding to bound ligands. However, the increases in the rate constants for O$_2$ dissociation from these LbaO$_2$ mutants are only 5-fold, as compared to the 200–500-fold increases observed for the Val^{E7} and Leu^{E7} replacements in sperm whale Mb. Thus, the hydrogen-bonding interaction between bound ligands and His^{E7} in wild-type Lba is significantly weaker than in Mb, presumably due to interactions with Tyr^{B10}.

In the absence of crystal structures of CO and O$_2$ complexes of soybean Lba, structural modeling was used to investigate possible interactions between Tyr^{B10} and His^{E7} that would explain the IR spectra of native and mutant LbaCOs and the rates of O$_2$ dissociation from the corresponding oxygenated complexes. In the crystal structure of acetate-bound soybean metLba, Tyr^{B10} is much closer to His^{E7} than to the heme iron or the first two atoms of the bound ligand (*4*). The O atom of the Tyr^{B10} side chain is ~3.3 Å away from the edge of the imidazole ring of His^{E7} and >4.0 Å away from the second ligand atom. Even in the absence of a bound ligand, the phenol side chain cannot move closer to the iron atom unless there is substantial movement of the entire B helix toward the heme plane, and such a large-scale movement would also require significant movement of the E helix. However, the Tyr^{B10} and His^{E7} side chains both appear to be flexible enough to interact with each other while allowing only the E7 imidazole to interact directly with bound ligands.

The model shown in Figure 10A was generated from the acetate-bound metLba crystal structure (*4*) by using the "flipped" orientation of the E7 imidazole ring described by Mabbutt et al. (*37*, *38*) and then rotating both the His^{E7} and Tyr^{B10} side chains about their Cα–Cβ and Cβ–Cγ bonds in the program O without violating van der Waals restraints. In this conformation, the Nδ atom of His^{E7} can accept a hydrogen bond from the OH group of Tyr^{B10}, and the Nϵ–H group of His^{E7} can still donate a hydrogen bond to the bound ligand. This model predicts one His^{E7} conformer for the CO complex because only one orientation could be found that allows formation of a strong hydrogen bond between His^{E7} and both the Tyr^{B10} side chain and the bound ligand. In support of the model, the IR spectrum of LbaCO shows a single, narrow band with a peak at a slightly higher ν_{CO} than that for Mb. The model is also consistent with multiple ν_{CO} peaks in the IR spectra of Tyr^{B10} mutants of LbaCO because, in the absence of hydrogen bonding to the phenol side chain, His^{E7} is "free" to adopt other orientations.

The model in Figure 10A requires a 180° rotation of the His^{E7} side chain about the Cβ–Cγ bond compared to the orientation reported for the metLba acetate (*4*) and nicotinate (*54*) crystal structures. As mentioned previously, this "flipped"

(A) Wild type LbaCO model   (B) Wild type MbCO structure   (C) Arg^{E7} LbaCO model
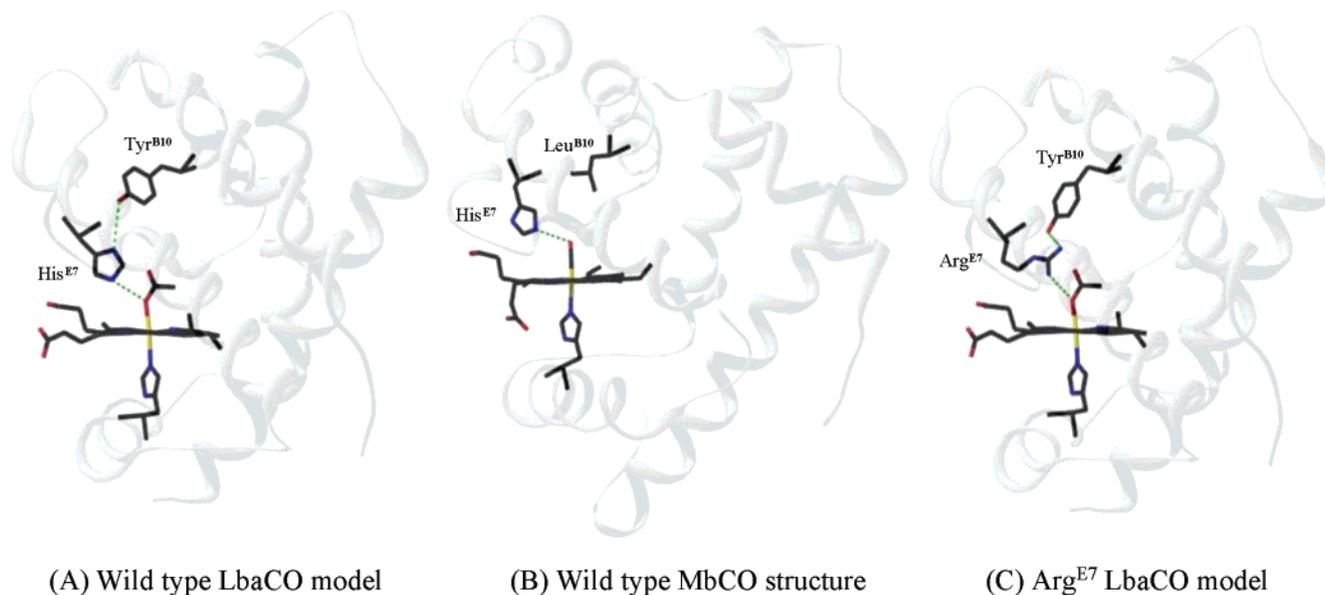
FIGURE 10: LbaCO model structures and wild-type MbCO. (A) Model for LbaCO. The acetomet-Lba structure (PDB entry 1BIN) was used as a starting point to explore possible interactions between Tyr^{B10} and His^{E7}, which would be consistent with the measured IR spectra, kinetic parameters, and NMR data (Tables 1 and 2; *37, 38, 53*). Minor changes to the side-chain torsion angles of these residues were made in the program *O*, allowing formation of a hydrogen bond between the Tyr^{B10} hydroxyl proton and the His^{E7} Nδ nonbonded electron pair. No highly unfavorable van der Waals overlaps were created in the process. The proposed hydrogen bonds are shown in green. (B) Crystal structure of MbCO (PDB 2MGK) (*11*). His^{E7} has more freedom of movement within the distal pocket of Mb to form an ideal hydrogen bond with the bound ligand than in the proposed Lba structure. (C) Model for Arg^{E7} LbaCO. His^{E7} was replaced with Arg in the program *O*, and then the rotomers for Tyr^{B10} and Arg^{E7} were searched until a terminal N atom of the guanidinium group was within hydrogen-bonding distance of the O atom of the Tyr^{B10} side chain. This model shows a possible conformation where the guanidinium group of Arg^{E7} is held inside the distal pocket with hydrogen bonds to the first or second ligand atom and the Tyr^{B10} side chain.

conformation is supported by NMR investigations by Wright's group, who showed that the imidazole ring of His^{E7} is oppositely oriented in LbaCO compared to that found in MbCO (*37, 38*). In solution, the Cϵ−H proton in Lba is closer to the heme than the Cδ−H proton, whereas the reverse is true in MbCO (*38*). The C−H proton resonances for the side chains of His^{E7} and Tyr^{B10} can be calculated using a combination of the program SHIFTS (*42*), the PDB files for the observed crystal structure, and the model in Figure 10A. These calculated chemical shifts can then be compared to those reported by Morikis et al. (*53*) for LbaCO.

The chemical shifts calculated for the His^{E7} Cβ protons in our model of LbaCO are 2.72 and 2.89 ppm and nearly identical to the values observed experimentally by Morikis et al. [2.73 and 2.88 ppm (*53*)]. The calculated Cβ−H shifts for the acetate−metLba structure are 3.26 and 3.27 ppm, indicating that the side chain is further from the heme plane when the larger acetate ligand is bound. More importantly, the predicted chemical shifts of the His^{E7} Cδ and Cϵ protons, 6.75 and 4.82 ppm, respectively, are much closer to the observed values of 7.15 and 5.26 ppm for LbaCO in solution than those calculated for acetate−metLba crystal structure, 7.04 and 8.11 ppm. The observed values for the His^{E7} Cδ and Cϵ protons require that the imidazole ring be rotated 180° with respect to the orientation found in the metLba (Figure 2) and sperm whale MbCO (Figure 10B) crystal structures (*37, 38*). The predicted chemical shifts of the Tyr^{B10} Cβ, Cγ, and Cδ protons for the model LbaCO structure (2.54, 3.00, 6.58, and 6.38 ppm) are also closer to the observed values [2.66, 2.42, 6.4, and 6.03 ppm (*53*)] than those calculated for the acetate−metLba crystal structure (2.79, 3.32, 7.09, and 6.69 ppm).

Thus, our structural interpretation in terms of direct hydrogen bonding between His^{E7} and Tyr^{B10} is consistent with all reported IR, ligand binding, and solution NMR data. However, more systematic modeling using molecular dynamics and energy minimization is needed. The ultimate verification of the model will come with NMR or crystal structure determinations of the wild-type LbaO$_2$ and LbaCO complexes.

The unusual properties of Arg^{E7} Lba can also be rationalized by a distal pocket structure similar to that proposed for the native protein (Figure 10C). In Lba, the guanidino group can potentially swing inward and form hydrogen bonds with both the phenol side chain of Tyr^{B10} and bound ligands. In the case of the relatively apolar FeCO complex, the interaction with the bound ligand is weak, and 15−20% of the population of mutant conformers has an apolar pocket with $\nu_{CO} \geq 1960$ cm^{-1}. However, in combination with the Tyr^{B10} side chain, the partial negative charge on the ligand atoms of the FeO$_2$ complex appears to cause Arg^{E7} to adopt a completely "in" conformation (Figure 10C). As a result, the Arg^{E7} mutation in LbaO$_2$ causes a 30-fold decrease in k_{O2}, producing a protein with ultrahigh O$_2$ affinity ($P_{50} \leq 1$ nM; Table 2).

Physiological Importance of the B10 Amino Acid. The role of the B10 amino acid in regulating ligand binding in Hbs is now widely accepted (*43, 55, 56*). As described in this work, the naturally occurring Tyr^{B10} side chain in soybean and cowpea Lb serves to "trap" His^{E7} in a single conformation that provides weaker stabilization to bound ligands than is observed in mammalian Mbs. This helps Lb maintain an oxygen affinity appropriate for its physiological function. In almost all mammalian Mbs and Hbs, the B10 residue is

a Leu. As a result, the distal pocket has significant "empty" space, and dissociated ligands can move easily toward the protein interior underneath the *sec*-butyl side chain, occupying what is called the "B" geminate state in laser photolysis experiments. This empty space adjacent to the bound ligand appears to be conserved to facilitate ligand capture and release in an otherwise relatively rigid protein structure. It may also be conserved to allow formation of the four-atom peroxynitrite intermediate that occurs during the dioxygenation of NO by bound O_2, a process that plays a key role in detoxifying NO in both myocytes and circulating blood (57−60). Introduction of Phe^{B10}, Tyr^{B10}, or Trp^{B10} into mammalian Mbs and Hbs fills this empty space, inhibiting the rate of both ligand binding and NO dioxygenation (60).

The presence of both His^{E7} and Tyr^{B10} in Hbs is unusual and appears to require a larger and more flexible active site. In the case of sperm whale Mb, the introduction of a Tyr at the B10 position leads to the formation of an unstable protein with kinetic heterogeneity and multiple ν_{CO} bands. When the distal His is replaced with more flexible amino acids in Mb double mutants, the Tyr^{B10} side chain appears to interact favorably with bound ligands (Figure 9; Table 2). Strong hydrogen bonds between bound ligands and Tyr^{B10} occur in many natural ultrahigh affinity Hbs, such as *Ascaris* Hb, and most of these proteins have Gln at the E7 position (13). *Ascaris* Hb resembles Lba in having a B10 Tyr, but it has a more compact distal heme pocket such that if Gln^{E7} is replaced with His, the resulting protein is hexacoordinated unlike wtLba (61). CO-bound *Ascaris* Hb also exhibits close proximity between the B10 phenolic proton and bound CO, suggesting that Tyr^{B10} in *Ascaris* Hb interacts directly with the bound ligand to increase affinity (61), whereas Tyr^{B10} in Lba has an indirect and destabilizing effect. Hence, variation in the positioning of the Tyr^{B10} as a function of E7 substitutions and the resulting alteration in the flexibility of distal heme pockets impart important physiological functions.

Correlations of CO IR Stretching Frequencies and Rate of O_2 Release by Lba. Phillips et al. (19) showed that there is a strong, inverse, linear correlation between the electrostatic field adjacent to bound CO and its stretching frequency. Recently, Franzen (32) has presented a more sophisticated analysis of the hydrogen-bonding and electrostatic potentials in these proteins. Both types of analyses demonstrate unequivocally that ν_{CO} is an inverse measure of the hydrogen-bonding potential and/or electric field adjacent to the bound ligand atoms. Low values of ν_{CO} correspond to positive electrostatic fields and strong hydrogen bond donation, whereas high values of ν_{CO} correspond to no hydrogen bonding and/or negative electrostatic fields.

Surprisingly, there is only a weak correlation between the average value of ν_{CO} and the rate of CO dissociation, primarily because the FeCO complex is relatively nonpolar and the variation in k_{CO} is small [≤30-fold between the various Mb and Lba mutants listed in Table 2 (18, 19)]. In contrast, a strong linear correlation is observed between the measured values of $\bar{\nu}_{CO}$ and the logarithm of the rate constant for O_2 dissociation (Figure 11; 19)), presumably because the FeO_2 complex is highly polar. A stabilizing positive electrostatic field and hydrogen-bonding potential provides a simple explanation for the 3000-fold variation in k_{O2} for Mb distal pocket mutants. A significantly poorer correlation ($r^2 = 0.50$) between $\bar{\nu}_{CO}$ and log (k_{O2}) is observed for the series
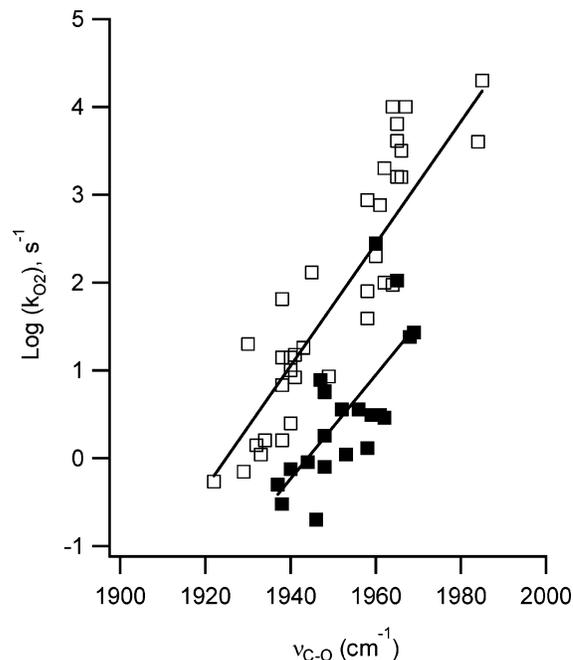

FIGURE 11: Correlation between the stretching frequencies of CO bound to wild-type Lba, Mb, various mutant proteins, and their corresponding oxygen dissociation rate constants. There is a strong linear correlation ($r^2 = 0.82$) between $\bar{\nu}_{CO}$ and log(k_{O2}) for the 31 different sperm whale Mbs (open squares), which are listed in Table 2 and described in Phillips et al. (19). A significant but poorer correlation ($r^2 = 0.50$) is observed between $\bar{\nu}_{CO}$ and log(k_{O2}) for the series of Lba mutants listed in Table 2 (solid squares).

of Lb mutants listed in Table 2 (Figure 11). The cause of the variance is flexibility of the distal pocket, particularly the conformation of the E7 side chain, which probably changes between the CO and O_2 complexes of Lba.

Arg^{E7} Lba provides a good example of large apparent differences between the O_2 and CO complexes. The IR spectrum of the CO complex shows conformational heterogeneity with a broad peak at moderately low frequency and another broad peak at moderately high frequency. Because $\bar{\nu}_{CO}$ is 1946 cm^{-1}, only a small decrease in k_{O2} is predicted. However, the observed rate constant decreases 30-fold, suggesting strongly that the Arg^{E7} side chain has completely swung into the distal pocket, stabilizing bound O_2 due to its partial negative charge (Figure 10C). A distal Arg side chain has been shown to stabilize bound oxygen in *Aplysia limacina* Mb (62) and in the DOS-oxygen sensor protein from *Bradyrhizobium japonicum*, which has a very low rate of O_2 dissociation (63).

The nearly parallel fitted lines in the plots of log(k_{O2}) versus ν_{CO} shown in Figure 11 demonstrate that the general electrostatic/hydrogen bonding mechanism for preferentially regulating O_2 dissociation applies to both Mb and Lba. The line is displaced in Lba probably due to proximal stabilization of ligand binding, causing lower k_{O2} values. The electrostatic mechanism and the proposed structure in Figure 10A explain qualitatively all of the large changes produced by distal pocket mutations in Lba. Replacement of the distal His with large apolar residues that exclude water from the distal pocket cause increases in ν_{CO} and k_{O2} (Table 2). Replacement of Tyr^{B10} with apolar amino acids causes the appearance of strong low-frequency ν_{CO} bands and decreases in k_{O2} (Table 2) because the distal His is free to adopt multiple conforma-

tions, some of which form strong hydrogen bonds with bound ligands. When both Tyr^{B10} and His^{E7} are replaced with apolar amino acids, the resulting Lba double mutant shows an IR spectrum identical to that of Mb with a hydrophobic distal pocket and a large O_2 dissociation rate constant.

ACKNOWLEDGMENT

REFERENCES

1. Appleby, C. (1974) in *The Biology of Nitrogen Fixation* (Quispel, A., Ed.), pp 521−544, North-Holland Publishing, Amsterdam, The Netherlands.

2. Wittenberg, J., Bergensen, F., Appleby, C., and Turner, G. (1974) Facilitated oxygen diffusion. The role of leghemoglobin in nitrogen fixation by bacteroids isolated from soybean root nodules, *J. Biol. Chem. 249*, 4057−4066.

3. Arutyunyan, É. G., Kuranova, I. P., Vainshtein, B. K., and Steigemann, W. (1980) X-ray structural investigation of leghemoglobin: VI. Structure of acetate-ferrileghemoglobin at a resolution of 2.0 Å, *Sov. Phys. Cryst. 25*, 43−58.

4. Hargrove, M. S., Barry, J. K., Brucker, E. A., Berry, M. B., Phillips, G. N., Jr., Olson, J. S., Arredondo-Peter, R., Dean, J. M., Klucas, R. V., and Sarath, G. (1997) Characterization of recombinant soybean leghemoglobin a and apolar distal histidine mutants, *J. Mol. Biol. 266*, 1032−1042.

5. Kundu, S., and Hargrove, M. S. (2003) Distal heme pocket regulation of ligand binding and stability in soybean leghemoglobin, *Proteins 50*, 239−248.

6. Kundu, S., Snyder, B., Das, K., Chowdhury, P., Park, J., Petrich, J. W., and Hargrove, M. S. (2002) The leghemoglobin proximal heme pocket directs oxygen dissociation and stabilizes bound heme, *Proteins 46*, 268−277.

7. Patel, N., Jones, D., and Raven, E. (2000) Investigation of the haem-nicotinate interaction in leghaemoglobin. Role of hydrogen bonding, *Eur. J. Biochem. 267*, 2581−2587.

8. Kundu, S., Trent, J. T., III, and Hargrove, M. S. (2003) Plants, humans, and hemoglobins, *Trends Plant Sci. 8*, 387−393.

9. Chowdhury, P., Kundu, S., Halder, M., Das, K., Hargrove, M. S., and Petrich, J. W. (2003) Effects of distal pocket mutations on the geminate recombination of NO with leghemoglobin on the picosecond timescale, *J. Phys. Chem. B 107*, 9122−9127.

10. Takano, T. (1977) Structure of myoglobin refined at 2.0 Å resolution: II. Structure of deoxymyoglobin from sperm whale, *J. Mol. Biol. 110*, 569−584.

11. Quillin, M. L., Arduini, R. M., Olson, J. S., and Phillips, G. N., Jr. (1993) High-resolution crystal structures of distal histidine mutants of sperm whale myoglobin, *J. Mol. Biol. 234*, 140−155.

12. Barrick, D. (1994) Replacement of the proximal ligand of sperm whale myoglobin with free imidazole in the mutant His-93→Gly, *Biochemistry 33*, 6546−6554.

13. Draghi, F., Miele, A., Travaglini-Allocatelli, C., Vallone, B., Brunori, M., Gibson, Q., and Olson, J. (2002) Controlling ligand binding in myoglobin by mutagenesis, *J. Biol. Chem. 277*, 7509−7519.

14. Olson, J. S., and Phillips, G. N., Jr. (1997) Myoglobin discriminates between O_2, NO, and CO by electrostatic interactions with the bound ligand, *J. Biol. Inorg. Chem. 2*, 544−552.

15. Springer, B. A., Sligar, S. G., Olson, J. S., and Phillips, G. N., Jr. (1994) Mechanisms of ligand recognition in myoglobin, *Chem. Rev. 94*, 699−714.

16. Caughey, W. S., Alben, J. O., McCoy, S., Boyer, S. H., Carache, S., and Hathaway, P. (1969) Differences in the infrared stretching frequency of carbon monoxide bound to abnormal hemoglobins, *Biochemistry 8*, 59−62.

17. Sage, J. T., Morikis, D., and Champion, P. M. (1991) Spectroscopic studies of myoglobin at low pH: heme structure and ligation, *Biochemistry 30*, 1227−1237.

18. Li, T., Quillin, M. L., Phillips, G. N., Jr., and Olson, J. S. (1994) Structural determinants of the stretching frequency of CO bound to myoglobin, *Biochemistry 33*, 1433−1446.

19. Phillips, G. N. J., Teodoro, M. L., Li, T., Smith, B., and Olson, J. S. (1999) Bound CO is a molecular probe of electrostatic potential in the distal pocket of myoglobin, *J. Phys. Chem. B 103*, 8817−8829.

20. Ray, G. B., Li, X.-Y., Ibers, J. A., Sessler, J. L., and Spiro, T. G. (1994) How far can proteins bend the FeCO unit? Distal polar and steric effects in heme proteins and models, *J. Am. Chem. Soc. 116*, 162−176.

21. Shimada, H., and Caughey, W. S. (1982) Dynamic protein structures: Effects of pH on conformer stabilities at the ligand-binding site of bovine heart myoglobin carbonyl, *J. Biol. Chem. 257*, 11893−11900.

22. Ansari, A., Berendzen, J., Braunstein, D., Cowen, B. R., Frauenfelder, H., Hong, M. K., Iben, E. T., Johnson, J. B., Ormos, P., Sauke, T. B., Scholl, R., Schulte, A., Steinbach, P. J., Vittitow, J., and Young, R. D. (1987) Rebinding and relaxation in the myoglobin pocket, *Biophys. Chem. 26*, 337−355.

23. Ormos, P., Braunstein, D., Frauenfelder, H., Hong, M. K., Lin, S.-L., Sauke, T. B., and Young, R. D. (1988) Orientation of carbon monoxide and structure−function relationship in carbonmonoxymyoglobin, *Proc. Natl. Acad. Sci. U.S.A. 85*, 8492−8496.

24. Decatur, S. M., and Boxer, S. G. (1995) A test of the role of electrostatic interactions in determining the CO stretch frequency in carbonmonoxymyoglobin, *Biochem. Biophys. Res. Commun. 212*, 159−164.

25. Potter, W. T., Hazzard, J. H., Choc, M. G., Tucker, M. P., and Caughey, W. S. (1990) Infrared spectra of carbonyl hemoglobins: Characterization of dynamic heme pocket conformers, *Biochemistry 29*, 6283−6295.

26. Frauenfelder, H., Parak, F., and Young, R. D. (1988) Conformational substates in proteins, *Annu. Rev. Biophys. Chem. 17*, 451−479.

27. Hong, M. K., Braunstein, D., Cowen, B. R., Frauenfelder, H., Iben, I. E., Mourant, J. R., Ormos, P., Scholl, R., Schulte, A., Steinbach, P. J., Xie, A.-H., and Young, R. D. (1990) Conformational substates and motions in myoglobin: External influences on structure and dynamics, *Biophys. J. 58*, 429−436.

28. Johnson, J. B., Lamb, D. C., Frauenfelder, H., Muller, J. D., McMahon, B., Nienhaus, G. U., and Young, R. D. (1996) Ligand binding to heme proteins. VI. Interconversion of taxonomic substates in carbonmonoxymyoglobin, *Biophys J. 71*, 1563−1573.

29. Li, X.-Y., and Spiro, T. G. (1988) Is bound CO linear or bent in heme proteins? Evidence from resonance Raman and infrared spectroscopic data, *J. Am. Chem. Soc. 110*, 6024−6033.

30. Oldfield, E., Guo, K., Augspurger, J. D., and Dykstra, C. E. (1991) A molecular model for the major conformational substates in heme proteins, *J. Am. Chem. Soc. 113*, 7537−7541.

31. Park, K. D., Guo, K., Adebodun, F., Chiu, M. L., Sligar, S. G., and Oldfield, E. (1991) Distal and proximal ligand interactions in heme proteins: Correlations between C−O and Fe−C vibrational frequencies, oxygen-17 and carbon-13 nuclear magnetic resonance chemical shifts, and oxygen-17 nuclear quadrupole coupling constants in $C^{17}O$- and ^{13}CO-labeled species, *Biochemistry 30*, 2333−2347.

32. Franzen, S. (2002) An electrostatic model for the frequency shifts in the carbonmonoxy stretching band of myoglobin: correlation of hydrogen bonding and the stark tuning rate, *J. Am. Chem. Soc. 124*, 13271−13281.

33. Spiro, T. G., and Kozlowski, P. M. (1998) Discordant results on FeCO deformability in heme proteins reconciled by density functional theory, *J. Am. Chem. Soc. 120*, 4524−4525.

34. Makinen, M. W., Houtchens, R. A., and Caughey, W. S. (1979) Structure of carboxymyoglobin in crystals and in solution, *Proc. Natl. Acad. Sci. U.S.A. 76*, 6042−6046.

35. Caughey, W. S., Shimada, H., Miles, G. C., and Tucker, M. P. (1981) Dynamic protein structures: infrared evidence for four discrete rapidly interconverting conformers at the carbon monoxide binding site of bovine heart myoglobin, *Proc. Natl. Acad. Sci. U.S.A. 78*, 2903−2907.

36. Fuchsman, W. H., and Appleby, C. A. (1979) CO and O_2 complexes of soybean leghemoglobins: pH effects upon infrared and visible spectra. comparisons with CO and O_2 complexes of myoglobin and hemoglobin, *Biochemistry 18*, 1309−1321.

37. Mabbutt, B., Appleby, C. A., and Wright, P. E. (1983) NMR studies of oxyleghemoglobin: Assignment of distal histidine proton resonances and evidence for pH-dependent changes in conformation, *Biochim. Biophys. Acta 749*, 281−288.

38. Mabbutt, B., and Wright, P. E. (1985) Assignment of heme and distal amino acid resonances in the ^{1}H-NMR spectra of the carbon

monoxide and oxygen complexes of sperm whale myoglobin, *Biochim. Biophys. Acta 832*, 175−185.

39. Arredondo-Peter, R., Moran, J. F., Sarath, G., Luan, P., and Klucas, R. V. (1997) Molecular cloning of the cowpea leghemoglobin II gene and expression of its cDNA in *Escherichia coli*. Purification and characterization of the recombinant protein, *Plant Physiol. 114*, 493−500.

40. Rohlfs, R. J., Mathews, A. J., Carver, T. E., Olson, J. S., Springer, B. A., Egeberg, K. D., and Sligar, S. G. (1990) The effects of amino acid substitution at position E7 (residue 64) on the kinetics of ligand binding to sperm whale myoglobin, *J. Biol. Chem. 265*, 3168−3176.

41. Jones, T., Zou, J., Cowan, S., and Kjeldgaard, M. (1991) Improved methods for building protein models in electron density maps and the location of errors in these models, *Acta Crystallogr. A47*, 110−119.

42. Xu, X.-P., and Case, D. A. (2002) Probing multiple effects on ^{15}N, ^{13}C alpha, ^{13}C beta and ^{13}C chemical shifts in peptides using density functional theory, *Biopolymers 65*, 408−423.

43. Carver, T. E., Brantley, R. E., Jr., Singleton, E. W., Arduini, R. M., Quillin, M. L., Phillips, G. N., Jr., and Olson, J. S. (1992) A novel site-directed mutant of myoglobin with an unusually high O_2 affinity and low autoxidation rate, *J. Biol. Chem. 267*, 14443−14450.

44. Springer, B. A., Egeberg, K. D., Sligar, S. G., Rohlfs, R. J., Mathews, A. J., and Olson, J. S. (1989) Discrimination between oxygen and carbon monoxide and inhibition of autoxidation by myoglobin. Site-directed mutagenesis of the distal histidine, *J. Biol. Chem. 264*, 3057−3060.

45. Shimada, H., Dong, A., Matsushima-Hibiya, Y., Ishimura, Y., and Caughey, W. S. (1989) Distal His→Arg mutation in bovine myoglobin results in a ligand binding site similar to the abnormal beta site of hemoglobin zurich (β63 His→Arg), *Biochem. Biophys. Res. Commun. 158*, 110−114.

46. Tucker, P. W., Phillips, S. E. V., Perutz, M. F., Houtchens, R., and Caughey, W. S. (1978) Structure of hemoglobins Zürich [His E7(63)β→Arg] and Sydney [Val E11(67)β→Ala] and role of the distal residues in ligand binding, *Proc. Natl. Acad. Sci. U.S.A. 75*, 1076−1080.

47. Quillin, M. L., Li, T., Olson, J. S., Phillips, G. N., Jr., Dou, Y., Ikeda-Saito, M., Regan, R., Carlson, M., Gibson, Q. H., Li, H., and Elber, R. (1995) Structural and functional effects of apolar mutations of the distal valine in myoglobin, *J. Mol. Biol. 245*, 416−436.

48. Lambright, D. G., Balasubramanian, S., Decatur, S. M., and Boxer, S. G. (1994) Anatomy and dynamics of a ligand-binding pathway in myoglobin: The roles of residues 45, 60, 64, and 68, *Biochemistry 33*, 5518−5525.

49. Smerdon, S. J., Dodson, G. G., Wilkinson, A. J., Gibson, Q. H., Blackmore, R. S., Carver, T. E., and Olson, J. S. (1991) Distal pocket polarity in ligand binding to myoglobin: Structural and functional characterization of a threonine^{68} (E11) mutant, *Biochemistry 30*, 6252−6260.

50. Sikorski, M. M., Topunov, A. F., Strozycki, P. M., Vorgias, C. E., Wilson, K. S., and Legocki, A. B. (1995) Cloning and expression of plant leghemoglobin cDNA of *Lupinus luteus* in *Escherichia coli* and purification of the recombinant protein, *Plant Sci. 108*, 109−117.

51. Gibson, Q. H., Wittenberg, J. B., Wittenberg, B. A., Bogusz, D., and Appleby, C. A. (1989) The kinetics of ligand binding to plant hemoglobins: structural implications, *J. Biol. Chem. 264*, 100−107.

52. Harutyunyan, E. H., Safonova, T. N., Kuranova, I. P., Popov, A. N., Teplyakov, A. V., Obmolova, G. V., Valnshtein, B. K., Dodson, G. G., and Wilson, J. C. (1996) The binding of carbon monoxide and nitric oxide to leghaemoglobin in comparison with other haemoglobins, *J. Mol. Biol. 264*, 152−161.

53. Morikis, D., Lepre, C. A., and Wright, P. E. (1994) ^1H resonance assignments and secondary structure of the carbon monoxide complex of soybean leghemoglobin determined by homonuclear two-dimensional and three-dimensional NMR spectroscopy, *Eur. J. Biochem. 219*, 611−626.

54. Ellis, P. J., Appleby, C. A., Guss, J. M., Hunter, W. N., Ollis, D. L., and Freeman, H. C. (1997) Structure of the ferric soybean leghemoglobin *a* nicotinate at 2.3 Å resolution, *Acta Crystallogr. D53*, 302−310.

55. Yang, J., Kloek, A., Goldberg, D., and Mathews, F. (1995) The structure of *Ascaris* hemoglobin domain I at 2.2 Å resolution: Molecular features of oxygen avidity, *Proc. Natl. Acad. Sci. U.S.A. 92*, 4224−4228.

56. Pesce, A., Dewilde, S., Kiger, L., Milani, M., Ascenzi, P., Marden, M., Hauwaert, M.-L. V., Vanfleteren, J., Moens, L., and Bolognesi, M. (2001) Very high-resolution structure of a trematode hemoglobin displaying a TyrB10-TyrE7 heme distal residue pair and high oxygen affinity, *J. Mol. Biol 309*, 1153−1164.

57. Eich, R. F., Li, T., Lemon, D. D., Doherty, D. H., Curry, S. R., Aitken, J. F., Mathews, A. J., Johnson, K. A., Smith, R. D., Phillips, G. N., Jr., and Olson, J. S. (1996) Mechanism of NO-induced oxidation of myoglobin and hemoglobin, *Biochemistry 35*, 6976−6983.

58. Doherty, D., Doyle, M. P., Curry, S. R., Vali, R., Fattor, T., Olson, J., and Lemon, D. (1998) The rate of reaction with NO determines the hypertensive effect of cell-free hemoglobin, *Nat. Biotechnol. 16*, 672−676.

59. Herold, S., Exner, M., and Boccini, F. (2003) The mechanism of the peroxynitrite-mediated oxidation of myoglobin in the absence and presence of carbon dioxide, *Chem. Res. Toxicol. 16*, 390−402.

60. Dou, Y., Maillett, D. H., Eich, R. F., and Olson, J. S. (2002) Myoglobin as a model system for designing heme protein based blood substitutes, *Biophys. Chem. 98*, 127−148.

61. Das, T. K., Samuni, U., Lin, Y., Goldberg, D. E., Rousseau, D. L., and Friedman, J. M. (2004) Distal heme pocket conformers of carbonmonoxy derivatives of *Ascaris* hemoglobin: Evidence of conformational trapping in porous sol−gel matrices, *J. Biol. Chem. 279*, 10433−10441.

62. Conti, E., Moser, C., Rizzi, M., Mattevi, A., Lionetti, C., Coda, A., Ascenzi, P., Brunori, M., and Bolognesi, M. (1993) X-ray crystal structure of ferric *Aplysia limacina* myoglobin in different liganded states, *J. Mol. Biol 233*, 498−508.

63. Dunham, C. M., Dioum, E. M., Tuckerman, J. R., Gonzalez, G., Scott, W. G., and Gilles-Gonzalez, M. A. (2003) A distal arginine in oxygen-sensing heme-PAS domains is essential to ligand binding, signal transduction, and structure, *Biochemistry 42*, 7701−7708.

BI049848G